



# pH treatment on the optical and structural properties of niobium vanadium pentoxide nanoparticles for optoelectronics and energy storage applications

A. A. Ibiyemi<sup>a,\*</sup>, J. I. Lawal<sup>b</sup>, S. K. Aminu<sup>a</sup>, A. G. Adewole<sup>a</sup>, B. M. Akinroye<sup>a,c</sup>, A. C. Adeniran<sup>c</sup>, O. A. Abulude<sup>c</sup>

<sup>a</sup>Department of Physics, Federal University Oye-Ekiti, Ekiti State, Nigeria

<sup>b</sup>Department of Physics, University of Ilesa, Osun State, Nigeria

<sup>c</sup>Department of Physics, Osun State College of Technology, Esa Oke, Osun State, Nigeria

## Abstract

In this work, vanadium pentoxide is doped with niobium (Nb) particles using co-precipitation technique and effect of pH in alkaline medium was examined. The impact of pH on the optical, chemical, luminescence, morphological and structural characteristics of Niobium intercalated into vanadium pentoxide made by precipitation technique is disclosed. XRD technique was used to examine the structural properties such as interplanar spacing of the samples. The high interplanar spacing of 5.7835 Å obtained at pH 12 show that NbV<sub>2</sub>O<sub>5</sub> sample can be used in energy storage device due to its large spacing. The energy band gap is decreased with increasing pH. The energy band gap for Nb-V<sub>2</sub>O<sub>5</sub> samples generated at pH 8, 10, and 12 are 2.70, 2.50, and 2.30 eV. At approximately 680 nm, NbV<sub>2</sub>O<sub>5</sub> nanoparticles revealed the emission of red light at all pH. One of the most important factors in improving the optical properties and crystallinity of nanostructured niobium doped vanadium oxide is lowering the pH level of the media. These nanostructures have great promise for the advancement of technological applications, particularly in the areas of UV filtering due to high absorbance revealed within the UV wavelength range. Niobium-doped Vanadium oxide nanoparticle is presently discovered as one of the storage device due to its large Interplanar spacing of 5.7835 Å at pH 12.

DOI:10.46481/asr.2025.4.2.310

**Keywords:** pH, Precipitation, Alkaline, Vanadium, Niobium

## Article History :

Received: 20 April 2025

Received in revised form: 04 June 2025

Accepted for publication: 10 June 2025

Published: 29 June 2025

© 2025 The Author(s). Published by the Nigerian Society of Physical Sciences under the terms of the Creative Commons Attribution 4.0 International license. Further distribution of this work must maintain attribution to the author(s) and the published article's title, journal citation, and DOI.

## 1. Introduction

One important characteristic affecting vanadium's behavior in a variety of applications, including energy storage, is its interplanar spacing, especially in vanadium pentoxide. The distance between parallel atomic planes in a crystal structure is known as interplanar spacing. Intercalation, which involves inserting additional molecules or ions between the layers to create enlarge space have high tendency of changing the interplanar spacing in vanadium pentoxide. Because of its high interplanar spacing, which influences its ion transport and electrical conductivity, vanadium pentoxide is a layered material that can be used effectively in energy storage devices.

\*Corresponding author: Tel. No.: +234-915-858-4828.

Email address: [abideen.ibiyemi@fuoye.edu.ng](mailto:abideen.ibiyemi@fuoye.edu.ng) (A. A. Ibiyemi)

The method of intercalation modifies the interplanar spacing and other characteristics of vanadium pentoxide by inserting foreign materials between its layers. Expanded interplanar space can improve the performance of energy storage devices like batteries and ease ion transport, making it a crucial modification for a variety of applications, including energy storage [1–4].

The 21st century has seen an unprecedented demand for clean energy and fuels due to the ever-increasing need for sustainable energy, environmental protection, and electrification of the entire transportation system. This has necessitated a rapid advancement in the development of large-scale, cost-effective, and efficient energy storage systems. Safe, dependable, effective, and reasonably priced energy storage solutions are required because of the sharp increase in energy consumption and the significant transition from conventional fossil fuels to renewable energy [1, 2]. One really interesting option to achieve this seems to be the use of energy storage device like aqueous ion batteries [3, 4]. The nontoxicity, low cost, environmental friendliness, excellent safety, and high ionic conductivity of aqueous batteries such as Zn-ion batteries make it to be more beneficial over the organic counterparts [5]. The high abundance of zinc and the less redox potential are some of the unique advantages of zinc metal anode that have made aqueous Zn-ion batteries stand out among others [5, 6]. The slow  $\text{Zn}^{2+}$  ion transport in cathode materials, which results from the large atomic mass and divalent state of zinc ion material, is one of the main challenges impeding aqueous Zn-ion batteries development. This leads to the suboptimal cycling stability and rate performance [7] which may have a negative impact on the cathode materials' structural stability and the reversibility of the redox processes, leading to a poor rate performance and insufficient energy efficiency of the Zn-ion batteries [5, 6]. The promising cathode materials for flexible solid state Zn-ion batteries are organic redox-active chemicals, which have poor rate capabilities and low electrical conductivities [8, 9]. Presently, more research is being done on materials having two-dimensional layered structures, such as those based on vanadium [10–15], which can facilitate rapid charge-carrier diffusion [16, 17]. The most attractive cathode options for aqueous Zn-ion batteries at the moment are layered vanadium pentoxide ( $\text{V}_2\text{O}_5$ ) due to their open structure, large interplanar spacing, which facilitates easy ion transport, and their ability to conduct multielectron transfer [17]. The hydrated vanadium oxide is the most promising of  $\text{V}_2\text{O}_5$  and its derivatives because of its quick ion-exchange capabilities, mixed valence states ( $\text{V}^{5+}$  and  $\text{V}^{4+}$ ), and enlarged interlayer spacing ( $\sim 11.5\text{\AA}$ ) [18, 19].

The easiest and most efficient way to stabilize the layered structure is by pre-intercalating foreign ions [20]. Several species, such as transition metals ( $\text{Ag}^+$ ,  $\text{Co}^{2+}$ ,  $\text{Cu}^{2+}$ ,  $\text{Zn}^{2+}$ ), alkali ( $\text{Li}^+$ ,  $\text{Na}^+$ ,  $\text{K}^+$ ), alkali earth ( $\text{Ca}^{2+}$ ,  $\text{Mg}^{2+}$ ), and other ions or groups ( $\text{NH}_4^+$ ), have been investigated to adjust the interlayer spacing and chemical composition of vanadium pentoxide [21–25], but  $\text{Nb}^{2+}$  has not been tested. The metal ion-preintercalated vanadium oxides have greater capacity retention and higher specific capacities [26–28]. The factors influencing the interlayer spacing of metal ion-preintercalated vanadium oxides and the causes of the optimal  $\text{Zn}^{2+}$  in storage characteristics have not been thoroughly examined, despite the widespread usage of the pre-intercalation method.

In this investigation, coprecipitation technique was used to create vanadium pentoxide intercalated with Niobium ion. The Nb-pre-intercalated vanadium pentoxide was then synthesized at different alkaline pH, this was done to establish the effect of pH on Nb-pre-intercalated vanadium pentoxide. By simply substituting some interlayer molecules,  $\text{Nb}^{2+}$  ions can be intercalated into the vanadium pentoxide structure, maintaining the bilayered structure with increasing the interplanar distance from  $4.363\text{\AA}$  ( $\text{V}_2\text{O}_5$ ) [29] to  $5.7835\text{\AA}$  ( $\text{NbV}_2\text{O}_5$ ). The reported interplanar spacing when different metal ions such as Na, Mn, Mg, K and Ni were intercalated into vanadium pentoxide layer are  $9.34\text{\AA}$  [30],  $10.3\text{\AA}$  [31],  $13.4\text{\AA}$  [32],  $10.4\text{\AA}$  [33] and  $11.4\text{\AA}$  [21], respectively. The interplanar spacing of vanadium oxide as reported by He et al, is  $4.363\text{\AA}$ , but when niobium was intercalated into vanadium pentoxide, the interplanar spacing enlarged to  $5.7835\text{\AA}$  at pH 12. At low alkaline pH, the interplanar spacing is  $5.4845\text{\AA}$  and  $5.5643\text{\AA}$  at pH 10. The interplanar spacing is increased with increasing pH. It shows that the interplanar spacing of niobium vanadium pentoxide can be more enlarged at high alkaline pH. The optical, chemical, photoemission, morphology and structural characteristics of niobium doped vanadium oxide nanoparticles made using the precipitation method were analysed.

The results of this study show that the pH of the solution is one of the primary factors that must be controlled during synthesis in order to significantly impact the material properties of  $\text{NbV}_2\text{O}_5$ . It also demonstrates that one of the main determinants that significantly affects the material properties and need to be managed during synthesis is the pH of the solution. The synthesis solution's pH (alkalinity) have impact on the particles' size, shape, optical characteristics, and surface morphology [22, 23, 34]. The pH is considered to have a significant impact since the rate at which ions dissociate and react to generate  $\text{NbV}_2\text{O}_5$  is closely linked to hydroxide ions ( $\text{OH}^-$ ), an oxygen source. To create high-quality crystals with improved optical and morphological properties, the pH of the solutions was adjusted. Since hydroxide ions ( $\text{OH}^-$ ) are intimately related to the rate at which ions dissociate and react to form  $\text{NbV}_2\text{O}_5$ , data indicate that pH has a major effect. All of the measurements in this work show that increasing the alkalinity of the synthesis solution enhanced the development of highly crystalline Nb-doped  $\text{V}_2\text{O}_5$  nanostructures, which is a better and more suitable material for the field of solar cells and other optoelectronics applications.

## 2. Methodology

### 2.1. Materials and method

$\text{NbV}_2\text{O}_5$  nanoparticles were created using the chemical co-precipitation method. The starting components for the current study are ammonia ( $\text{NH}_3$ ) solution, sodium hydroxide ( $\text{NaOH}$ ), niobium chloride and vanadium nitrate hexahydrate. Niobium chloride ( $\text{NbCl}_3$ ), vanadium nitrate hexahydrate ( $\text{V}(\text{NO}_3)_3 \cdot 6\text{H}_2\text{O}$ ) and sodium hydroxide ( $\text{NaOH}$ ) in an aqueous solution in deionized water were combined to create the solution medium. Using a computerized weighing balance, the necessary weight of the compounds'

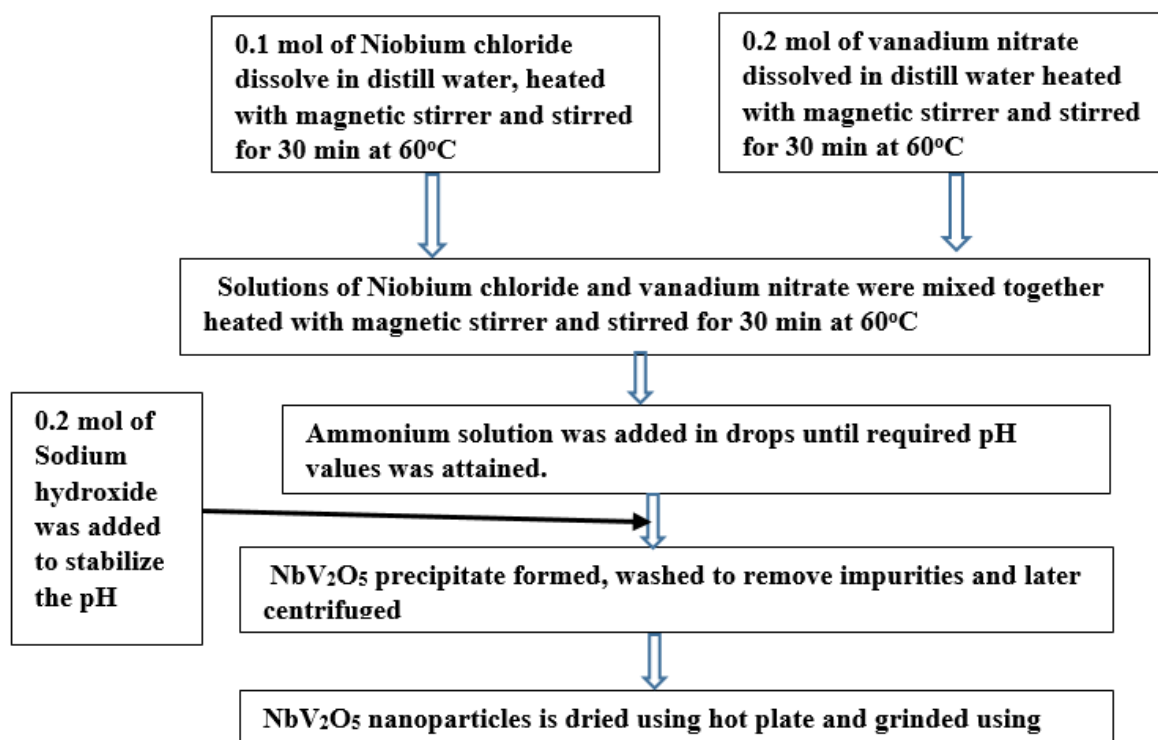


Figure 1: Schematic diagram of experimental procedure of niobium vanadium pentoxide nanoparticles.

aqueous solution was calculated. 0.1 mol of Niobium chloride and 0.2 mol of vanadium nitrate hexahydrate  $V(NO_3)_2 \cdot 6H_2O$  were dissolved in 500 ml of distilled water and heated using a magnetic stirrer. The solution was then kept under constant stirring to completely dissolve Niobium chloride and vanadium nitrate hexahydrate  $V(NO_3)_2 \cdot 6H_2O$  for one hour. After full dissolution, 0.2 mol solution of sodium hydroxide was added which was then constantly stirred. The reaction was allowed to proceed for one hour after complete addition of ammonia solution and the attainment of required pH values (8, 10 and 12). Drop by drop, ammonia solution was added until pH values of 8, 10, and 12 were reached, which helps the precipitate to form. The solution was centrifuged for 10 min and the supernatant was discarded. After removing undesired particles by washing with deionized water, the precipitated nanoparticles were dried on a hot plate. The samples of nanoparticles were ground to produce fine particles in powdery form.

## 2.2. Characterization

The optical properties such as transmittance and absorbance of the nanoparticles were examined using UV-Vis spectrophotometer (Jasco-V-570 Spectrophotometer, Japan), surface morphology were examined using Scanning Electron Microscope (FEG JEOL JSM-7800). The structural characteristics were examined by employing X-ray diffraction technique (Rigaku powder X-ray Diffractometer Ruker Advanced D8 model with  $CuK\alpha$  radiation  $\lambda = 1.5406 \text{ \AA}$ ) and the atomic composition were formed using Energy Dispersive X-ray Spectroscopy (Quantax 200 with X Flash e Bruker). Figure 1 shows the schematic diagram of the experimental procedure.

## 3. Results and discussion

### 3.1. X-ray diffraction analysis of the $NbV_2O_5$ nanoparticles

Using the XRD method, particle structure and lattice parameters were investigated after the acquisition of niobium-doped vanadium oxide nanoparticles. An X-ray diffractometer was also used to examine the powder's phase. Monochromatic  $CuK\alpha$  radiation ( $\lambda = 1.54056 \text{ \AA}$ ) acting at 40 kV tube voltage was used for XRD. With a step size of  $0.02^\circ$ , the sample was scanned from  $0^\circ$  to  $70^\circ$  at a diffraction angle of  $2\theta$ . As a result, niobium-doped vanadium oxide nanoparticles XRD profiles for pH 8, pH 10, and pH 12 were acquired and are displayed in Figures 2. Every niobium-doped vanadium oxide nanoparticles sample's diffraction peak precisely correlates with the  $V_2O_5$  listed on the JCPDF card (No. 9015662). The pattern suggests that  $NbV_2O_5$  samples with varying solution pHs are composed of orthorhombic structure and Shcherbinaite phase with a preferential diffraction plane orientation (101). The remarkable purity of the produced compounds was evidenced by the lack of additional peaks in the XRD pattern, which would have indicated the presence of extra impurities or contaminants. The niobium-doped vanadium oxide nanoparticles samples' broadening

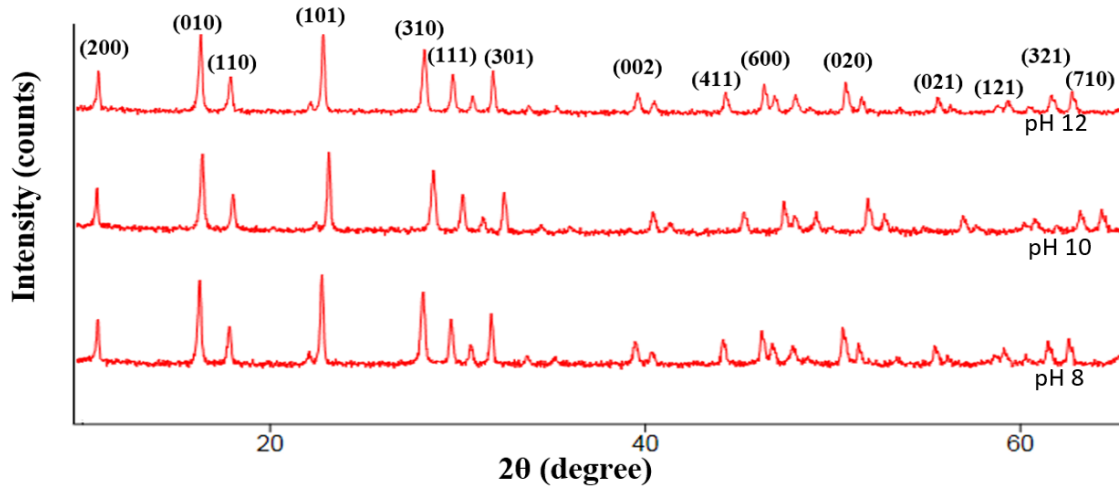


Figure 2: Diffraction pattern of niobium-doped vanadium oxide nanoparticles synthesized in alkaline media.

Table 1: Niobium doped vanadium oxide nanoparticle crystallite sizes and lattice constants obtained at various pH levels.

pH	D (nm)	a (Å)	c (Å)	V (Å <sup>3</sup> )	$\delta$ (linm <sup>-2</sup> )	$\epsilon$ (lin <sup>-2</sup> m <sup>-4</sup> )	Interplanar spacing (Å)
8	21.672	11.3581	4.5729	589.9335	0.00212	0.0627	5.4845
10	18.556	11.5752	4.7039	630.2532	0.00294	0.01071	5.5643
12	9.718	11.8548	4.7527	667.9267	0.01058	0.00285	5.7835

diffraction peaks show a high level of crystallinity and the presence of tiny particles [35]. It was discovered that each peak fit the standard's diffracted image quite well. Compared to the other niobium-doped vanadium oxide nanoparticles peaks, the (101) reflection had a significantly higher intensity. From the XRD analysis, a shcherbinaite phased vanadium oxide was formed at all pH levels. Shcherbinaite is a mineral which comprises vanadium and oxide as its chemical components. The fine crystallite size of the niobium-doped vanadium oxide particles is shown by the broad peaks in XRD patterns. The data from X-ray diffraction were used to calculate the interplanar spacing [28].

A niobium-doped vanadium oxide sample produced at pH 12 demonstrated a highest interplanar spacing of 4.8789 Å. Niobium-doped vanadium oxide nanoparticles is henceforth useful as a good storage material because of its great interplanar spacing. The volume of the unit cell was determined using  $V = a^2c$ , the crystallite size was determined using  $D = \frac{K\lambda}{\beta \cos \theta}$  and lattice constant were determined using  $\frac{1}{d^2} = \frac{h^2+k^2}{a^2} + \frac{l^2}{c^2}$ , where  $\theta$  is the Bragg's diffraction angle,  $\lambda$  is the X-ray wavelength,  $\beta$  is the full width at half maximum (FWHM) in radians,  $D$  is the crystallite size,  $a$ ,  $c$  are the lattice constants and  $d$  is the distance between the planes that correspond to the Miller indices  $h$ ,  $k$ ,  $l$ . Table 1 displays the computed lattice constants and crystallite size at different alkaline pH. The average crystallite size of the synthesized nanoparticles was calculated and discoverer that, due to quantum confinement, the crystallite sizes shrank to quantum dot size as pH levels rose to 12. It has already been demonstrated that raising the pH decreases crystallite size. pH has an impact on nanoparticle size [20]. Smaller crystallite sizes of the nanoparticles are frequently the outcome of raising the pH of the fluid during production. This is due to the fact that pH affects how quickly the nanoparticles precipitate and aggregate, which can have an impact on the final particle size [23, 35]. When the pH level reached 12, a quantum size particle was subsequently produced, and the unit cell's volume was also increased. The outcomes indicate that there was a slight increase in the lattice parameters, going from a value of  $a = 11.3581$  Å for pH 8 to 11.8548 Å for pH 12, and from a value of  $c = 4.5729$  Å for pH 8 to 4.7527 Å for pH 12. The estimated lattice constants nearly match the values reported in the literature, and no significant fluctuation in the lattice features at varied pH values is revealed.

The existence of nanocrystalline domains within the Niobium-doped vanadium oxide nanoparticles is shown by the sharpness of the diffraction peaks. Furthermore, the sharp and narrow peaks confirmed that Niobium-doped vanadium oxide nanoparticles had well crystallized. The dislocation density, was calculated by calculating the reciprocal of square of the crystallite size of diffraction peak. Stress and strain forces in crystal structure lead to a rise in dislocations and physical flaws. Consequently, table 1 displays the dislocations density, which is often referred to as the number of specimen flaws. Optimal crystallinity requires a low dislocation density, and a low value obtained by a sample at low pH indicates improved crystallinity. Low pH results in a decreasing dislocation density value, which promotes the increase of particle size [24]. Micro strain, which decreased from 0.00212 to 0.01058 by reducing the crystallite size, indicates the decrease in lattice defects of the nanoparticles.

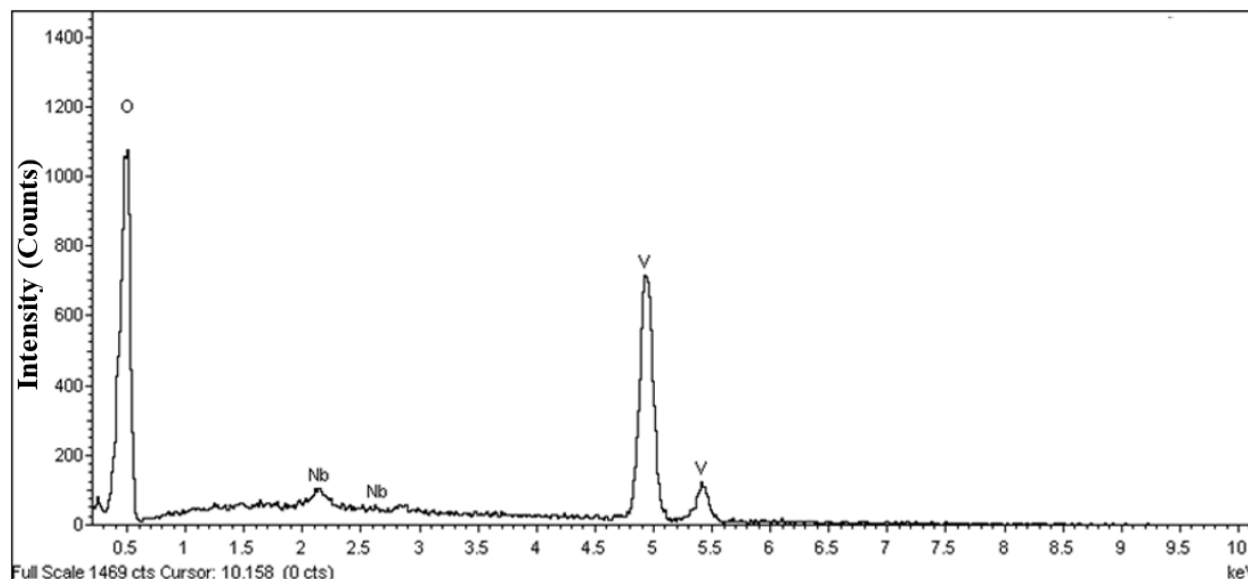


Figure 3: Spectral depicting the energy dispersive X-ray spectroscopy of niobium-doped vanadium oxide samples.

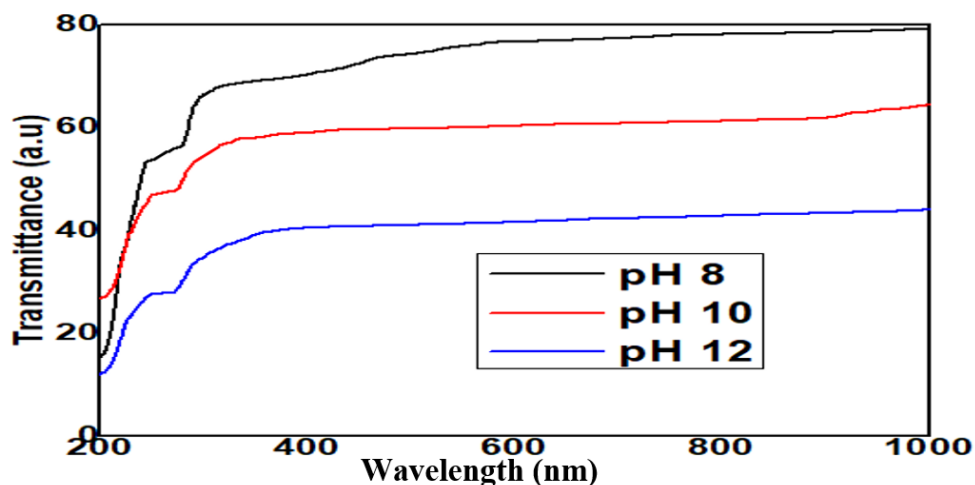


Figure 4: Transmittance of niobium-doped vanadium oxide samples synthesized at pH 8, 10 and 12.

### 3.2. Elemental dispersive spectroscopy of the $NbV_2O_5$ nanoparticles

The elemental composition of the generated compounds was ascertained using the widely utilized analytical technique known as Elemental Dispersive X-ray Spectroscopy (EDS). The EDS spectra of the generated compound is displayed in Figure 3. The only elementary species identified in the sample are Niobium (Nb), vanadium (V) and oxygen (O). In addition to the oxygen (O) and niobium (Nb) peaks at 0.5 Kev and 2.1 Kev, the peaks at 5.0 Kev and 5.5 Kev are responsible for the binding energies of vanadium (V). Vanadium, niobium and oxygen were thus present in the nanoparticles in pure samples, according to EDX. No additional peaks in the sample are associated with any other components. Therefore, the treated products are considered pure and uncontaminated. In terms of energy spectrum,  $Nb^{2+}$  and  $V^{5+}$  belongs to the L-series, whereas  $O^{2-}$  belongs to the K-series. Since no foreign elements (impurities) were detected by the EDS, the synthesized nanoparticles are 100% pure. It has been found that the results are consistent with XRD diffraction analysis. The appropriate stoichiometry and the EDS data agree fairly well. The EDS revealed the absence of foreign element (impurity), this shows that the synthesized nanoparticles is 100% pure.

### 3.3. Optical characteristics of niobium doped vanadium oxide

#### 3.3.1. Transmittance of niobium doped vanadium oxide

Figure 4 shows the transmittance of niobium-doped vanadium oxide samples produced at various pH values.  $Nb-V_2O_5$  nanoparticles produced at pH 8 show higher percentage transparency in the visible and infrared parts of the electromagnetic spectrum. When

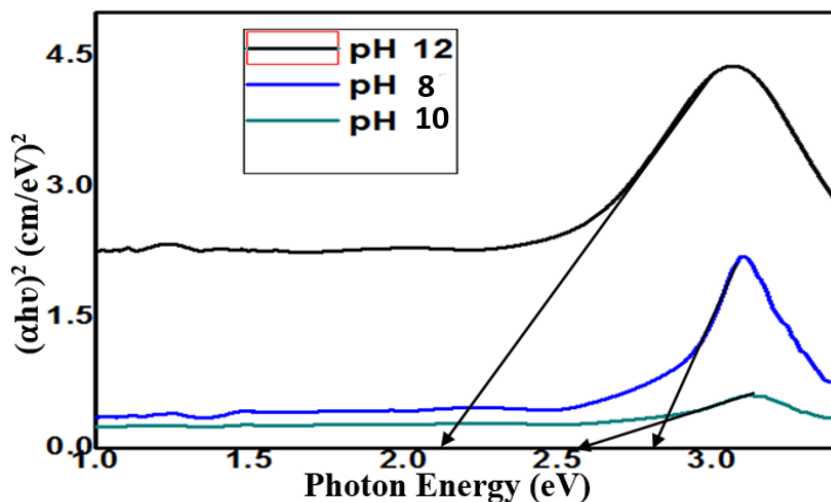


Figure 5: Optical energy band of niobium-doped vanadium oxide samples synthesized at pH 8, 10 and 12.

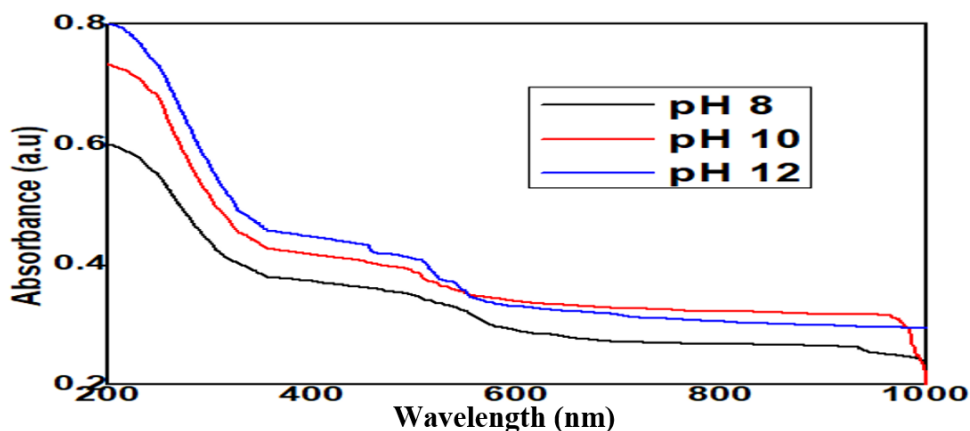


Figure 6: Absorbance of niobium-doped vanadium oxide samples synthesized at pH 8, 10 and 12.

the particles are synthesized at pH 12, a low percentage transmittance of around 40% is created inside the visible region; when Nb-V<sub>2</sub>O<sub>5</sub> samples is synthesized at pH 8, a maximum percentage transmittance of roughly 78% is produced. For varying pH levels of 8, 10, and 12, the percentage transmittance values of each sample are 78%, 58%, and 40%, respectively as shown in Figure 4. Similar result was reported by Ashraf et al. Because many optical charge carriers, or electrons, are produced at low pH values and add new energy levels to the energy band, the Nb-V<sub>2</sub>O<sub>5</sub> sample synthesized at pH 8 exhibits improved transparency. A larger percentage of transmittance is also a result of the sample produced at pH 8 having a higher quantity of charged particles and electron transfers from the valence band to the conduction band. The pH 8-produced Nb-V<sub>2</sub>O<sub>5</sub> sample is suitable for the production of efficient optoelectronic devices and may now be used to improve the window layer construction process for solar cell applications. The sample synthesized at a lower pH level reveals a slight optical loss, while the sample created at a higher pH level produces a significant optical loss. For every sample, higher percentage transmittances are generated in the infrared spectrum. The results show that samples of Nb-V<sub>2</sub>O<sub>5</sub> are more transparent to infrared light, implying that Nb-V<sub>2</sub>O<sub>5</sub> material could be utilized to develop the perfect material for the detection of infrared radiation.

### 3.3.2. Optical energy band gap of niobium doped vanadium oxide

The Tauc analogy is based on energy-dependent absorption coefficient  $\alpha$  which is represented by the equation (1): The approach for accurately calculating semiconductors' optical band gap energy using UV-Vis spectroscopy is Tauc method. The linear portion of the optical spectrum is typically directly extrapolated to the horizontal axis of the Tauc plot.

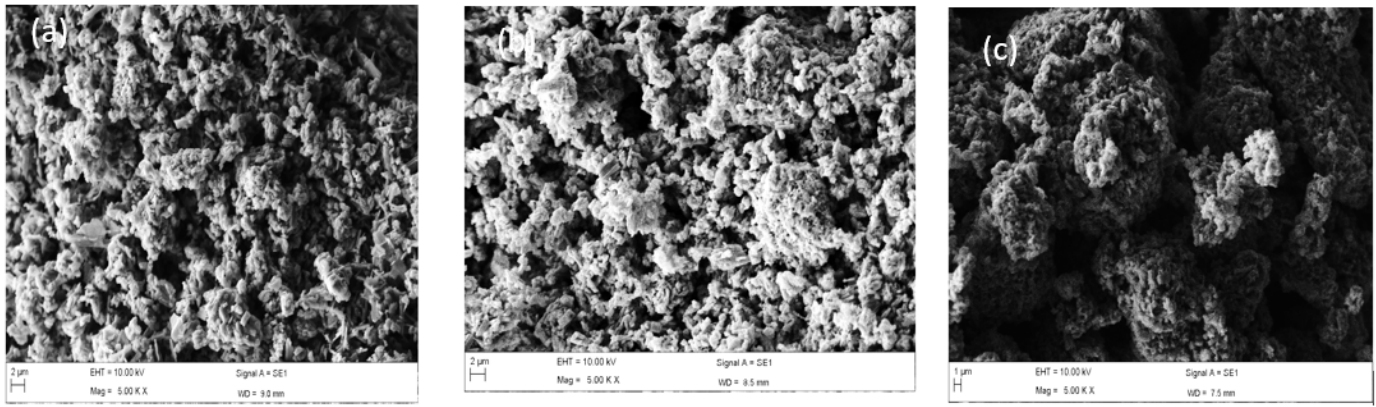


Figure 7: Surface morphology of niobium-doped vanadium oxide samples synthesized at pH (a) 8 (b) 10 and (c) 12.

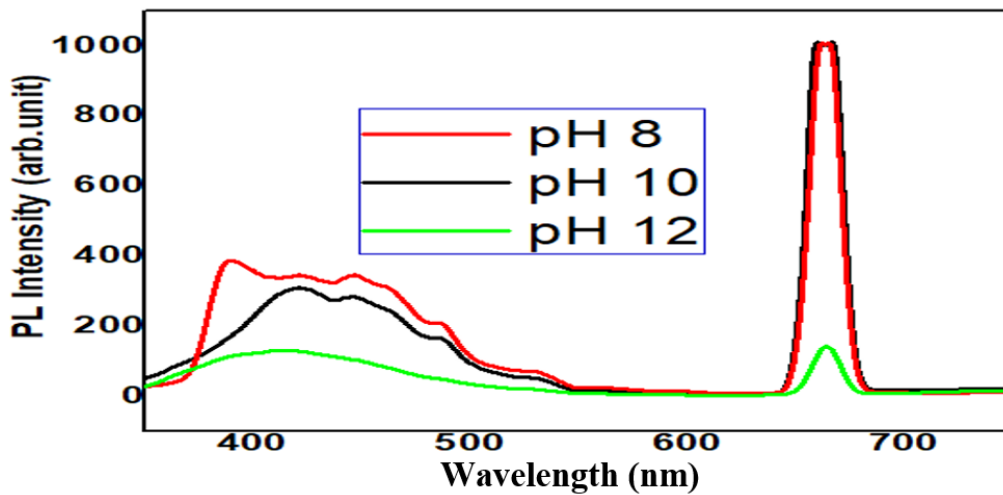


Figure 8: Photoluminescence spectral of niobium-doped vanadium oxide samples synthesized at pH 8, 10 and 12.

$$(\alpha h\nu) = A(h\nu - E_g)^n, \quad (1)$$

where  $A$  is a constant,  $h$  is the Planck constant,  $\nu$  is the photon's frequency, and  $E_g$  is the band gap's energy. Depending on the kind of electron transition, the  $n$  factor is either  $1/2$  for direct transition band gaps or  $2$  for indirect transition band gaps. Plotting  $(\alpha h\nu)^n$  against photon energy ( $h\nu$ ) allows one to estimate the optical band gap energy for both direct and indirect transitions. Extrapolating to  $(h\nu)^2 = 0$  for the direct transition yields the value of  $E_g$ .

The linear route of the spectra lines is extrapolated to find the energy band gap [36]. From Figure 5, the energy band gap shifted from 2.30 to 2.70 eV, suggesting that changes in pH were the cause of the band gap fluctuations. However, the physical state of Nb-V<sub>2</sub>O<sub>5</sub> sample is altered when the pH of the alkaline solution is altered. A pH change causes a shift in the energy band. When a Nb-V<sub>2</sub>O<sub>5</sub> sample is synthesized at pH 8, a wider band gap of about 2.70 eV is achieved. The energy band gap for Nb-V<sub>2</sub>O<sub>5</sub> samples generated at pH 8, 10, and 12 is 2.70, 2.50, and 2.30 eV. Energy band gap values clearly show that Nb-V<sub>2</sub>O<sub>5</sub> nanoparticles have a lesser variety of optoelectronic applications than ZnO and TiO<sub>2</sub> nanoparticles, particularly when utilized as solar cell window layers. The degree of optical absorption is mostly dependent on particle size; as pH increases, smaller particles have lower  $E_g$  values. Consequently, the size of the particles affects Nb-V<sub>2</sub>O<sub>5</sub> nanoparticles' capacity to absorb UV radiation. The huge  $E_g$  that fluctuates at room temperature is the most important feature in the utilization of Nb-V<sub>2</sub>O<sub>5</sub> and other semiconductor oxides like TiO<sub>2</sub> and ZnO in optoelectronics. Changes in the particle size and crystal structure also affect the band gap energy, which is the minimum energy needed to excite an electron from the valence band to the conduction band; for instance, a decrease in crystallite size brought on by a higher pH resulted in a decrease in the band gap energy. Changes in the pH also affected the nanoparticles' UV-visible absorption spectrum, causing a shift in the absorption peak, which is related to the band gap [23].

### 3.3.3. Optical absorption of niobium doped vanadium oxide

The absorbance bands of Nb-V<sub>2</sub>O<sub>5</sub> nanoparticles produce are displayed in Figure 6. The blue-shifted absorption edge's center ranges from 200 to 220 nm. UV radiation was significantly absorbed by Nb-V<sub>2</sub>O<sub>5</sub> sample, which also had a prominent absorption peak position at 200 nm. In the UV spectra, there was an absorption band observable at 200 nm. The findings demonstrated that the high transparency of V<sub>2</sub>O<sub>5</sub> nanoparticles produced at alkaline pH 8 to photon energy was the reason for the low absorption. The nanoparticle sample synthesized at pH 12 has a higher absorbance than Nb-V<sub>2</sub>O<sub>5</sub> samples produced at pH 8 and 10. Nb-V<sub>2</sub>O<sub>5</sub> samples having an elevated optical absorption edge in the ultraviolet spectrum can be used efficiently with UV detectors. Saleem *et al.* [25] and Arshad *et al.* [36], reported findings that were similar. Since Nb-V<sub>2</sub>O<sub>5</sub> nanoparticles produced at pH 12 can detect, absorb, and filter UV radiation that could cause interior home systems to heat up, they are now a viable option for UV management in architectural windows and UV photodetectors. Because of its superior UV absorption, this substance is a better compound for managing UV radiation.

### 3.4. Surface morphology of NbV<sub>2</sub>O<sub>5</sub> nanoparticles at different alkaline pH.

Scanning electron microscopy (SEM) was used to investigate the microstructural characteristics of Nb-V<sub>2</sub>O<sub>5</sub> nanoparticles. Grain size, pore dispersion, and surface roughness were investigated as surface and structural properties of the material. The SEM images of the Nb-V<sub>2</sub>O<sub>5</sub> crystalline structure at pH values of 8, 10, and 12 were displayed in Figure 7(a-c). After a comprehensive SEM micrograph investigation, it was found to be relatively thick and free of cracks. On SEM pictures, porosity and grain development pattern were clearly seen. The porous structure is seen to be prominent at pH level 12. At pH 8, Figure 7(a) shows the development of a densely packed structure and spheroid nano-grains with fair porosity; however, when pH changes, the density and compactness change. A non-homogeneity at the surface layer is indicated by the presence of surface defects such as voids at the surface morphology. The morphology is observed to be more homogeneous at pH 8 with spherically shaped grains that are more compacted and densely packed; at pH 10, the homogeneity fades. Low surface defects, such as pores, holes, and cavities, are evident in the surface morphology of the Nb-V<sub>2</sub>O<sub>5</sub> samples produced at pH 8, and the surface arrangement indicated the presence of big particle aggregation. The morphologies show the emergence of low compactness and low tightly packed spherical structure at pH 10 and pH 12. The presence of contaminants and distortion at the lattice site may be the cause of the significant aggregation seen in the Nb-V<sub>2</sub>O<sub>5</sub> sample synthesized at pH 12.

### 3.5. Luminescence of NbV<sub>2</sub>O<sub>5</sub> nanoparticles in alkaline solutions

The luminescence effect of niobium vanadium oxide samples was examined using photoluminescence spectroscopy. Figure 8 illustrates how strong emission bands occur with low pH value in niobium vanadium oxide samples. High luminescence intensity was obtained as the pH value is decreased in the alkaline solution. Weak emission was derived at high pH. The creation of oxygen vacancies in the niobium vanadium oxide lattice and the presence of donor energy levels close to the conduction band edge are thought to be the causes of the generation of strong luminescence peaks at low pH level 8 [37]. The sample synthesized at pH 12 revealed weak luminescence peak, this seems that the sample synthesized at pH 12 exhibit no oxygen vacancies in its lattice. Samples synthesized at pH 8 and 10 formed a prominent emission peak, which is attributable to the electron transfer from the donor level to the acceptor level. Particle size distribution have an impact on the expansion of emission bands with pH. The luminescence peaks go from lower to higher energy levels in location. The non-shift in the emission bands could be due the absence of an impurity level in the niobium vanadium oxide lattice. Red emission is formed by the synthesized samples at all pH. When blue and green emissions occur, the emission maxima at wavelengths of 450 nm and 510 nm move from a higher energy level to a lower energy level. At wavelength range 380 nm and 450 nm, a synthetic niobium vanadium oxide sample produces violet emissions.

## 4. Conclusions

This study used the co-precipitation approach to dope vanadium pentoxide with niobium (Nb) particles and investigated the impact of pH in an alkaline medium. The effects of pH on the morphological, structural, optical, chemical, and luminescence properties of Niobium-doped Vanadium oxide produced by precipitation process are revealed. Interplanar spacing and other structural characteristics of the samples were examined using the XRD technique. The NbV<sub>2</sub>O<sub>5</sub> sample can be utilized in energy storage devices because of its huge spacing, as demonstrated by the high interplanar spacing of 5.7835 Å measured at pH 12. As pH rises, the energy band gap decreases. Nb-V<sub>2</sub>O<sub>5</sub> samples produced at pH values of 8, 10, and 12 have energy band gaps of 2.70, 2.50, and 2.30 eV, respectively. Red light was emitted by NbV<sub>2</sub>O<sub>5</sub> nanoparticles at about 680 nm for all pH values. Reducing the media's pH is one of the most crucial steps in enhancing the optical characteristics and crystallinity of nanostructured niobium-doped vanadium oxide. Because of their high absorbance within the UV wavelength region, these nanostructures have considerable promise for the development of technological applications, especially in the fields of UV filtering and infrared detectors. The niobium-doped Vanadium oxide nanoparticle's high interplanar spacing of 5.7835 Å at pH 12 has led to its current discovery as a storage device. The interplanar spacing of vanadium oxide is 4.363 Å. However, at pH 12, the interplanar spacing increased to 5.7835 Å when niobium was intercalated into vanadium pentoxide. The interplanar spacing is 5.4845 Å at alkaline pH 8 and 5.5643 Å at pH 10. As the pH rises, the interplanar space increases.

## Data availability

Data will be made available upon reasonable request from the corresponding author.

## References

- [1] A. M. Omer, “Energy, environment and sustainable development”, *Renew. Sustain. Energy Rev.* **12** (2008) 2265. <https://doi.org/10.1016/j.rser.2007.05.001>.
- [2] J. Zhu, X. Chen & A. Q. Thang, “Vanadium-based metalorganic frameworks and their derivatives for electrochemical energy conversion and storage”, *Smart Mat.* **3** (2022) 384. <https://doi.org/10.1002/smm2.1091>.
- [3] T. Li, X. Peng & P. Cui, “Recent progress and future perspectives of flexible metal–air batteries”, *Smart Mat.* **2** (2021) 519. <https://doi.org/10.1002/smm2.1076>.
- [4] F. Li, Y. Li & J. Qu, “Recent developments of stamped planar micro-supercapacitors: materials, fabrication and perspectives”, *Nano Mater. Sci.* **3** (2021) 154. <https://doi.org/10.1016/j.nanoms.2020.10.003>.
- [5] X. Wu, R. Liu, J. Zhao & Z. Fan, “Advanced carbon materials with different spatial dimensions for supercapacitors”, *Nano Mater. Sci.* **3** (2021) 241. <https://doi.org/10.1016/j.nanoms.2021.01.002>.
- [6] X. Wang, J. Chai & J. Jiang, “Redox flow batteries based on insoluble redox-active materials: a review”, *Nano Mater. Sci.* **3** (2021) 17. <https://doi.org/10.1016/j.nanoms.2020.06.003>.
- [7] J. Zhang, M. Li, H. A. Younus, B. Wang, Q. Weng, Y. Zhang & S. Zhang, “An overview of the characteristics of advanced binders for high-performance Li-S batteries”, *Nano Mater. Sci.* **3** (2021) 124. <https://doi.org/10.1016/j.nanoms.2020.10.006>.
- [8] F. Wu, H. Yang, Y. Bai & V. Wu, “Paving the path toward reliable cathode materials for aluminum-ion batteries”, *Adv. Mater.* **31** (2019) 1806510. <https://doi.org/10.1002/adma.201806510>.
- [9] Y. Hu, D. Ye & B. B. Luo, “A binder-free and free-standing cobalt sulfide@carbon nanotube cathode material for aluminum-ion batteries”, *Adv. Mater.* **30** (2018) 1703824. <https://doi.org/10.1002/adma.201703824>.
- [10] M. C. Lin, M. Gong, B. Lu, Y. Wu, D. Y. Wang, M. Guan, M. Angell, C. Chen, J. Yang, B. J. Hwang & H. Dai, “An ultrafast rechargeable aluminium-ion battery”, *Nature* **520** (2015) 324. <https://doi.org/10.1038/nature14340>.
- [11] J. Sun, T. Wang, Y. Gao, Z. Pan, R. Hu & J. Wang, “Will lithium–sulfur batteries be the next beyond-lithium ion batteries and even much better?”, *InfoMat* **4** (2022) e12359. <https://doi.org/10.1002/inf2.12359>.
- [12] H. Hou, X. Qiu, W. Wei, Y. Zhang & X. Ji, “Carbon anode materials for advanced sodium-ion batteries”, *Adv. Energy Mater.* **7** (2017) 1602898. <https://doi.org/10.1002/aenm.201602898>.
- [13] K. Song, C. Liu, L. S. Mi, S. Chou, W. Chen & C. Shen, “Recent progress on the alloy-based anode for sodium-ion batteries and potassium-ion batteries”, *Small* **17** (2021) 1903194. <https://doi.org/10.1002/sml.201903194>.
- [14] W. Zong, H. Guo, Y. Ouyang, L. Mo, C. Zhou, G. Chao, J. Hofkens, Y. Xu, W. Wang, Y. E. Miao, G. He, I. P. Parkin, F. Lai & T. Liu, “Topochemistry-driven synthesis of transition-metal selenides with weakened van der Waals force to enable 3D-printed Na-ion hybrid capacitors”, *Adv. Funct. Mater.* **32** (2022) 2110016. <https://doi.org/10.1002/adfm.202110016>.
- [15] J. Zhou & S. Guo, “Carbon-based anode materials for potassium ion batteries: from material, mechanism to performance”, *Smart Mat.* **2** (2021) 176. <https://doi.org/10.1002/smm2.1042>.
- [16] Y. R. Pei, M. Zhao, Y. P. Zhu, C. C. Yang & Q. V. N. Jiang, “Nanoparticle-assembled hollow microspheres/N-doped carbon nanofibers: an anode material for superior potassium storage”, *Nano Mater. Sci.* **4** (2022) 104. <https://doi.org/10.1016/j.nanoms.2021.06.007>.
- [17] K. Zhu, T. Wu & K. A. Huang, “High-voltage activated high-performance cathode for aqueous Zn-ion batteries”, *Energy Storage Mater.* **38** (2021) 473. <https://doi.org/10.1016/j.ensm.2021.03.031>.
- [18] L. Wang, K.-W. Huang, J. Chen & J. Zheng, “Ultralong cycle stability of aqueous zinc-ion batteries with zinc vanadium oxide cathodes”, *Sci. Adv.* **5** (2019) eaax4279. <https://doi.org/10.1126/sciadv.aax4279>.
- [19] L. Chen, Z. Yang, F. Cui, J. Meng, H. Chen & X. Zeng, “Enhanced rate and cycling performances of hollow V2O5 nanospheres for aqueous zinc ion battery cathode”, *Appl. Surf. Sci.* **507** (2020) 145137. <https://doi.org/10.1016/j.apsusc.2019.145137>.
- [20] B. Gherbi, S. E. Laouini, S. Meneceur, A. Bouafia, H. Hemmami, M. L. Tedjani, G. Thiripuranathar, A. Barhoum & F. Mena, “Effect of pH value on the band gap energy and particles size for biosynthesis of ZnO nanoparticles: efficiency for photocatalytic adsorption of methyl orange”, *Sustain.* **14** (2022) 11300. <https://doi.org/10.3390/su141811300>.
- [21] J. Feng, Y. Wang, S. Liu, S. Chen, N. Wen, X. Zeng, Y. Dong, C. Huang, Q. Kuang & Y. Zhao, “Electrochemically induced structural and morphological evolutions in nickel vanadium oxide hydrate nanobelts enabling fast transport kinetics for high-performance zinc storage”, *ACS Appl. Mater. Interfaces* **12** (2020) 24726. <https://doi.org/10.1021/acsami.0c04199>.
- [22] M. Yalcin, “The effect of pH on the physical and structural properties of TiO2 nanoparticles”, *J. Cryst. Growth* **585** (2022) 126603. <https://doi.org/10.1016/j.jcrysgro.2022.126603>.
- [23] R. Ashraf, S. Riaz, S. S. Hussain & S. Naseem, “Effect of pH on properties of ZnO nanoparticles”, *Mater. Today: Proc.* **2** (2015) 5754. <https://doi.org/10.1016/j.matpr.2015.11.123>.
- [24] V. P. Prasadam, F. Bahlawane, G. Mattelaer, C. D. Rampelberg, L. Fang, Y. Jiang, K. Martens, I. P. Parkin & I. Papakonstantinou, “Atomic layer deposition of vanadium oxides: process and application review”, *Mater. Today Chem.* **12** (2019) 396. <https://doi.org/10.1016/j.mtchem.2019.03.004>.
- [25] S. Saleem, M. N. Ashiq, S. Manzoor, U. Ali, R. Liaqat, A. Algahtani, S. Mujtaba, V. Tirth, A. M. Alsuhaibani, M. S. Refat, A. Ali, M. Aslam & R. Zaman, “Analysis and characterization of opto-electronic properties of iron oxide (Fe2O3) with transition metals (Co, Ni) for the use in the photodetector application”, *J. Mater. Res. Technol.* **25** (2023) 6150. <https://doi.org/10.1016/j.jmrt.2023.07.065>.
- [26] Y. Liu, Y. An & L. Wu, “Interfacial chemistry modulation via amphoteric glycine for a highly reversible zinc anode”, *ACS Nano* **17** (2023) 552. <https://doi.org/10.1021/acsnano.2c09317>.
- [27] Y. Dai, X. Liao & R. Yu, “Quicker and more Zn<sup>2+</sup> storage predominantly from the interface”, *Adv. Mater.* **33** (2021) 2100359. <https://doi.org/10.1002/adma.202100359>.
- [28] J. Shin, D. S. Choi, H. J. Lee, Y. Jung & J. W. Choi, “Hydrated intercalation for high-performance aqueous zinc ion batteries”, *Adv. Energy Mater.* **9** (2019) 1900083. <https://doi.org/10.1002/aenm.201900083>.
- [29] P. He, G. Zhang & X. Liao, “Sodium ion stabilized vanadium oxide nanowire cathode for high-performance zinc-ion batteries”, *Adv. Energy Mater.* **8** (2018) 1702463. <https://doi.org/10.1002/aenm.201702463>.
- [30] H. Tian, Y. He, L. Wang, Y. Lai, J. Wang, H. Xiang, W. Zhao & L. Zhang, “Simultaneous pre-intercalation of caesium and sodium ions into vanadium oxide bronze nanowires for high-performance aqueous zinc-ion batteries”, *Mater. Chem. Front.* **6** (2022) 1920. <https://doi.org/10.1039/D2QM00420H>.
- [31] X. Pang, S. Ji, P. Zhang, W. Feng, L. Zhang, K. Li, Y. Tang & Y. Liu, “Interlayer doping of pseudocapacitive hydrated vanadium oxide via Mn<sup>2+</sup> for high-performance aqueous zinc-ion battery”, *Electrochim. Acta* **441** (2023) 141810. <https://doi.org/10.1016/j.electacta.2022.141810>.

- [32] F. Ming, H. Liang, Y. Lei, S. Kandambeth, M. Eddaoudi & H. N. Alshareef, "Layered Mg<sub>x</sub>V<sub>2</sub>O<sub>5</sub>·nH<sub>2</sub>O as cathode material for high-performance aqueous zinc ion batteries", *ACS Energy Lett.* **3** (2018) 2602. <https://doi.org/10.1021/acseenergylett.8b01423>.
- [33] Q. Li, X. Ye, H. Yu, C. Du, W. Sun, W. Liu, H. Pan & X. Rui, "Pre-potassiated hydrated vanadium oxide as cathode for quasi-solid-state zinc-ion battery", *Chin. Chem. Lett.* **33** (2022) 2663. <https://doi.org/10.1016/j.ccllet.2021.09.091>.
- [34] S. Castro-Lopes, Y. Guerra, A. Silva-Sousa, D. M. Oliveira, L. A. P. Gonçalves, A. Franco, E. Padrón-Hernández & R. Peña-García, "Influence of pH on the structural and magnetic properties of Fe-doped ZnO nanoparticles synthesized by sol gel method", *Solid State Sci.* **109** (2020) 106438. <https://doi.org/10.1016/j.solidstatesciences.2020.106438>.
- [35] L. Zhongshao, Z. Shuwen, S. Zewei, J. Hanxiang, H. Aibin, J. Ping & C. Xun, "Deterioration mechanism of vanadium dioxide smart coatings during natural aging: uncovering the role of water", *Chem. Eng.* **447** (2022) 137556. <https://doi.org/10.1016/j.ccej.2022.137556>.
- [36] S. Arshad, A. Hussain, S. Noreen, M. B. Tahir, J. Rehman, M. Jabeen, M. H. Benish & S. Rahman, "Structural, mechanical, electronic and optical properties of MFe<sub>2</sub>O<sub>4</sub> (M=Zn, Cu, Si) ferrites for electrochemical, photocatalytic and optoelectronic applications", *J. Solid State Chem.* **330** (2024) 124504. <https://doi.org/10.1016/j.jssc.2023.124504>.
- [37] A. A. Ibiyemi, A. Olusola & G. T. Yusuf, "Photoelectric and optoelectronic effects of hard ferromagnetic manganese cobalt (Mn-Co) ferrite nanoparticles for high frequency device application", *Appl. Phys. A: Mater. Sci. Process.* **128** (2022) 792. <https://doi.org/10.1088/1402-4896/ac4a95>.